**A&A manuscript no.**
(will be inserted by hand later)

**Your thesaurus codes are:**
**02.13.1, 11.03.1**

ASTRONOMY
AND
ASTROPHYSICS

# The temperature-mass relation in magnetized galaxy clusters

**Klaus Dolag**[1], **August Evrard**[2], **and Matthias Bartelmann**[1]

[1] Max-Planck-Institut für Astrophysik, P.O. Box 1317, D–85741 Garching, Germany
[2] Dept. of Physics, University of Michigan, Ann Arbor, MI 48109-1120, USA

**Abstract.** We use cosmological, magneto-hydrodynamic simulations of galaxy clusters to quantify the dynamical importance of magnetic fields in these clusters. The set-up of initial magnetic field strengths at high redshifts is chosen such that observed Faraday-rotation measurements in low-redshift clusters are well reproduced in the simulations. We compute the radial profiles of the intracluster gas temperature and of the thermal and magnetic pressure in a set of clusters simulated in the framework of an Einstein-de Sitter and a low-density, spatially-flat CDM cosmological model. We find that magnetic-field configurations which reproduce observed Faraday-rotation data in local clusters change the temperature of the intracluster gas changes by less than $\approx 5\%$.

**Key words:** Magnetic fields, Galaxies: clusters: general

## 1. Introduction

Magnetic fields are common in galaxy clusters. They are inferred from Faraday-rotation measurements (Vallee et al. 1986, 1987) in polarised background radio sources, and from diffuse radio haloes around galaxy clusters (Kronberg 1994). Depending on several assumptions, most notably on the characteristic length scale of field coherence, magnetic field strengths inferred from observations in typical galaxy cluster centres range from $\approx 0.1\mu$G up to some tens of $\mu$G.

Provided the magnetic field is tangled on sufficiently small scales for it to be considered randomised, it contributes a non-thermal pressure $p_{\rm B}$, which is related to the thermal pressure $p_{\rm th}$ through

$$\frac{p_{\rm B}}{p_{\rm th}} = 2.5\% \left(\frac{|\boldsymbol{B}|}{3\mu{\rm G}}\right)^2 \left(\frac{n}{10^{-3}\,{\rm cm}^{-3}}\right)^{-1} \left(\frac{T}{10^8\,{\rm K}}\right)^{-1} . \quad (1)$$

Conversely, magnetic fields ordered on scales comparable to the cluster scale can add anisotropic non-thermal pressure.

The structure of intracluster magnetic fields is unclear at present, and consequently the magnetic field strengths in clusters are equally uncertain. We investigate in this paper the amount of non-thermal pressure support due to realistic magnetic fields in simulated galaxy clusters.

Our approach is as follows (see Dolag et al. 1999 and 2000). We set up gas-dynamical cosmological cluster simulations at high redshift and impose magnetic fields of variable strength and structure as summarised in Table 2 below. Since the origin of magnetic fields on cluster scales is unknown, we use either completely homogeneous or chaotic initial magnetic field structures. The evolution of the intracluster fields is then computed during cluster collapse. The initial magnetic field strength (or energy density) is determined such that the simulated clusters at low redshift well reproduce the statistics of observed Faraday-rotation measurements taken from Kim et al. (1991). It turns out that (i) the initial field structure is irrelevant because the final field structure is completely determined by the dynamics of the cluster collapse, and (ii) initial field strengths of order $10^{-9}$ G at the initial redshift of the simulations (see Table 1) are adequate to reproduce the measured Faraday-rotation statistics.

*Send offprint requests to*: K. Dolag

## 2. Models

We use a set of ten numerically simulated galaxy clusters for investigating the effect of magnetic fields on the temperature and pressure stratification in these clusters. Here, we summarise the numerical technique only briefly because details on the methods applied, their implementation, and their performance in test problems have been published elsewhere (Dolag et al. 1999; hereafter DBL99).

### 2.1. GrapeMSPH

We use the cosmological MHD code described in DBL99 to simulate the formation of magnetised galaxy clusters from an initial density perturbation field. The code combines the merely gravitational interaction of a dark-matter component with the hydrodynamics of a gaseous component. The gravitational interaction of the particles is evaluated on GRAPE boards (cf. Sugimoto et al. 1990), while the gas dynamics is computed in the SPH approximation (Lucy 1977; Monaghan 1992). The original "GrapeSPH" code (Steinmetz 1996) was extended by adding the magneto-hydrodynamic equations to trace the evolution of the magnetic fields. Because of the assumed ideal electric conductivity, the fields are frozen into the gas flow. The back-reaction of the magnetic field on the gas via the Lorentz force is included.

Extensive tests of the code were performed and described in DBL99. The code succeeds in solving the co-planar MHD Riemann problem posed by Brio & Wu (1988). Although the simulated magnetic field is not strictly divergence-free, $\nabla \cdot \boldsymbol{B}$ is always negligible compared to the magnetic field divided by a typical length scale of $\boldsymbol{B}$ (see DBL99 for details). The code also assumes the intracluster medium to be an ideal gas with an adiabatic index of $\gamma = 5/3$, and neglects cooling. The surroundings of the clusters are important because their tidal fields affect the overall cluster structure and the merger history of the clusters. Therefore, the cluster simulation volumes are surrounded by a layer of boundary particles whose purpose it is to accurately represent the tidal fields of the cluster neighbourhood. Here we specially focus on the dynamical influence of the magnetic field in galaxy clusters, e.g. on the pressure support and the temperature in the clusters.

### 2.2. Initial conditions

We set up cosmological initial conditions for two CDM-dominated universes (EdS and FlatLow) as specified in Table 1. For each cosmology, we calculate ten different realisations of the initial density-fluctuation field at redshift $z_{\rm ini}$, which result in clusters of different final masses and dynamical states at redshift $z = 0$. We simulate each of these clusters with up to five different initial magnetic field configurations, listed in Table 2, yielding a total of 90 cluster models. A detailed description of these models (final magnetic field structure, strengths and a comparison with rotation measures) will be given in Dolag et al. (2000).

**Table 1.** Parameters of the EdS and the FlatLow models.

| model | $H_0$ | $\Omega_0$ | $\Lambda$ | $\sigma_8$ | $f_{\rm baryon}$ | $z_{\rm ini}$ |
|---|---|---|---|---|---|---|
| EdS | 0.5 | 1.0 | 0.0 | 1.2 | 5% | 15 |
| FlatLow | 0.7 | 0.3 | 0.7 | 1.05 | 10% | 20 |

As mentioned before, our previous work showed that information on the initial structure of the magnetic field is entirely lost during cluster collapse. The final field structures at low redshifts resulting either from a homogeneous or a chaotic initial field are statistically equivalent when compared to Faraday-rotation observations. This can also be seen in Figure 1, where it is shown that the pressure support does not depend on the initial field structure. We can therefore focus here on the homogeneous set-up of the initial field, which is numerically easier to handle.

One major point of the previous study (DBL99) was the statistics of synthetic Faraday-rotation measurements along random lines-of-sight through simulated clusters, and its comparison to the observed rotation-measure statistics. It was found there that the *medium* initial magnetic field strength could reproduce the observed statistics very well. The simulated and the observed rotation-measure distributions could not significantly be distinguished in a Kolmogorov-Smirnov test. However, the scatter in both measurements and simulations is large. This is due to the low number of simulated clusters per set, and to the selection criteria of galaxy clusters involved in the simulations and the observations. We therefore allow for a range of initial magnetic field strengths which results in a range of synthetic Faraday-rotation distributions which are still well in agreement with the observed data. Choosing a realistic model to distribute relativistic electrons in the simulated clusters, the simulations are also able to match the properties of observed radio-haloes very well, including the observed very steep relation between cluster temperature and radio luminosity (see Dolag & Ensslin 2000).

**Table 2.** Initial magnetic fields (column 2) and the resulting final magnetic field strengths in the simulated clusters (column 3 and 4 for EdS and FlatLow models, respectively). The final values are an average of the magnetic field over the central region (within a radius of 350 kpc) and over all ten clusters for each cosmology.

| initial field | $B_{\rm ini}$ | $\langle B_{\rm final}\rangle^{\rm EdS}_{\rm core}$ | $\langle B_{\rm final}\rangle^{\rm FlatLow}_{\rm core}$ |
|---|---|---|---|
| no | 0.0 G | — | — |
| low (chaotic) | $0.2 \times 10^{-9}$ G | $0.4\ \mu$G | — |
| low | $0.2 \times 10^{-9}$ G | $0.4\ \mu$G | $0.3\ \mu$G |
| medium | $1.0 \times 10^{-9}$ G | $1.1\ \mu$G | $0.8\ \mu$G |
| high | $5.0 \times 10^{-9}$ G | $2.5\ \mu$G | $2.0\ \mu$G |

### 2.3. Quantities calculated

The correlation length of final magnetic field configurations near cluster centres is of order $50\ \rm kpc$ (see DBL99). Field orientations in regions large compared to the correlation length can therefore be considered as randomised. For instance, there is no preferred direction in the final magnetic pressure distribution. Thus, we can safely average thermodynamic quantities like the gas pressure and gas temperature in spherical shells, provided these shells are sufficiently thick compared to the field correlation length.

The radial distances to the cluster centres are scaled by the virial radius $r_{200}$. For simulated clusters, $r_{200}$ is defined as the radius enclosing a mean density $\bar\rho(r_{200})$ of 200 times the critical density $\rho_{\rm cr}$,

$$\bar\rho(r_{200}) = \frac{3M(r_{200})}{4\pi\, r_{200}^3} = 200\,\rho_{\rm cr}\ . \qquad (2)$$

The temperature profiles give mass-weighted temperatures averaged in shells, divided by the mass-weighted temperatures in the shell at the radius $r_{200}$ of the corresponding non-magnetised cluster.

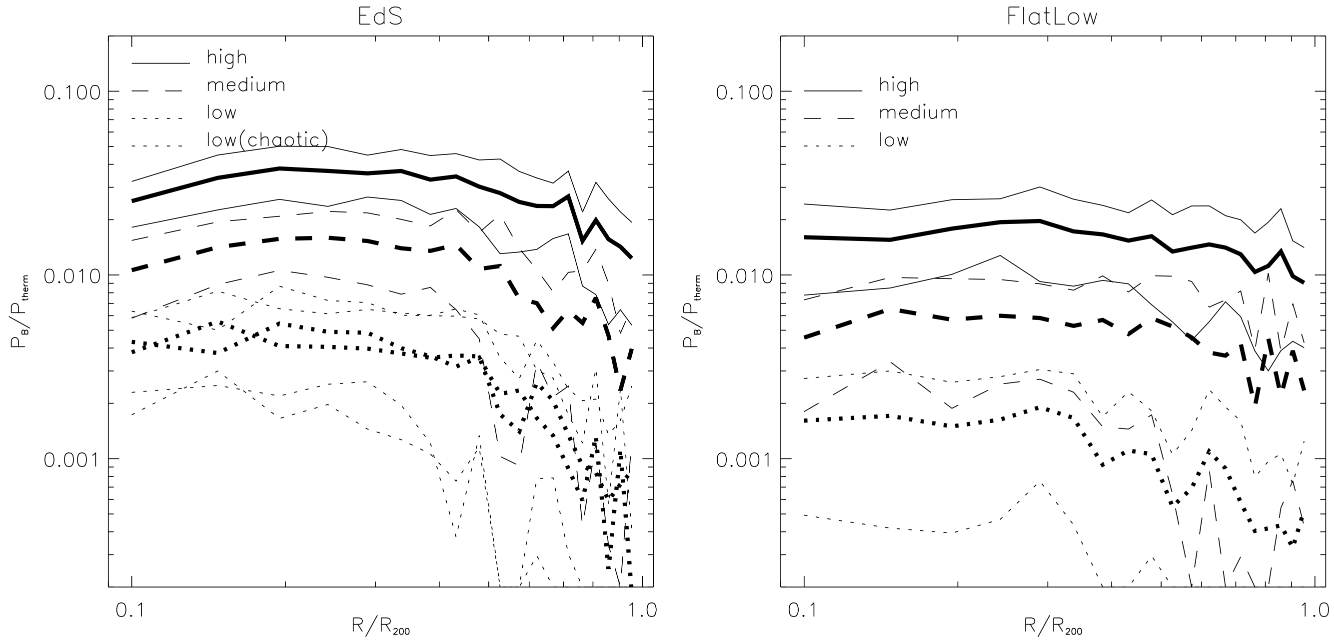


**Fig. 1.** Shown here is the ratio between the magnetic and the thermal pressure in shells around the cluster centre as a function of radius in units of the virial radius $r_{200}$ (heavy lines). Different line types distinguish the different initial magnetic field strengths as indicated in the plot. The two dotted lines represent the low field with homogeneous and with chaotic initial field configurations. Both lead to the same amount of pressure support in the final clusters. The curves show the average across the entire simulated cluster sample. The thin lines indicate the *rms* scatter within the sample. Near cluster centres, the ratio between magnetic and thermal pressure is consistent with the isotropic estimate of eq. (1). The left panel represents the realisations for the EdS cosmology, the right panel for the FlatLow cosmology.

## 3. Results

During cluster formation and evolution, the simulated intracluster magnetic field strengths are amplified by compression, tangling and bending of field lines, and shear flows in the gas. The magnetic field structure is also affected by merging, accretion of sub-clumps, and consequent relaxation processes. In combination, these processes amplify the initial magnetic fields in the simulation by factors of order $\approx 1000$. If initial field strengths are chosen such that final fields of $\mu$G strength are reached in and near cluster cores, the observed statistics of Faraday-rotation measurements is well reproduced. The growing magnetic fields affect the balance between the gravitational force and the total (magnetic plus thermal) pressure during cluster formation.

### 3.1. Radial structure

On the whole, the near isotropic magnetic pressure has the tendency to counteract gas collapse, and therefore acts in a similar manner as the thermal pressure. This implies that the gas stratification can achieve hydrostatic equilibrium at lower temperature, because lower thermal pressure is required in presence of the additional pressure support due to the magnetic field. Figure 1 shows, averaged in shells, the ratio

$$\mathcal{F}_{\rm p}(R) = \frac{p_{\rm B}(R)}{p_{\rm th}(R)} = \frac{\left\langle |\boldsymbol{B}|^2/8\pi \right\rangle_{R_1 \le R \le R_2}}{\left\langle p_{\rm th} \right\rangle_{R_1 \le R \le R_2}} \tag{3}$$

between the magnetic pressure $p_{\rm B}$ and the thermal pressure $p_{\rm th}$ as a function of the radius $R$. Due to compression and turbulence in the gas flow, the magnetic field is highest in and near the centres of the simulated clusters, where the thermal pressure is also highest. As Fig. 1 shows, the relative contribution of magnetic fields to the pressure support appears to peak somewhere between the cluster core radii and the virial radii $r_{200}$. This feature, however, is not very pronounced, so that the ratio between magnetic and thermal pressure support is almost constant across a large range of cluster-centric radii. Due to the smaller final masses of the clusters in the FlatLow cosmology, the magnetic pressure support is also smaller in these clusters. Nevertheless, these less magnetized clusters are able to match the observed Faraday-rotation. This is because the value of $H_0$ is chosen higher in the low-density universe, so that the projected, physical distances of the measurement locations with respect to the cluster centre shrink. Closer to the cluster centre, the magnetic field is generally higher, and therefore these less magnetised clusters well reproduce the measurements.

The overall structure of the magnetic field in the outer regions of the clusters differs from that near the cluster centre. Accretion and merger events arrange the magnetic fields in the outer cluster regions in coherent patterns on fairly large scales. Near the cluster centre, the gas flow pattern is almost randomised, and the magnetic field is consequently tangled and bent on fairly small scales. Although the magnetic pressure can be considered isotropic at or near the cluster centre, it may well

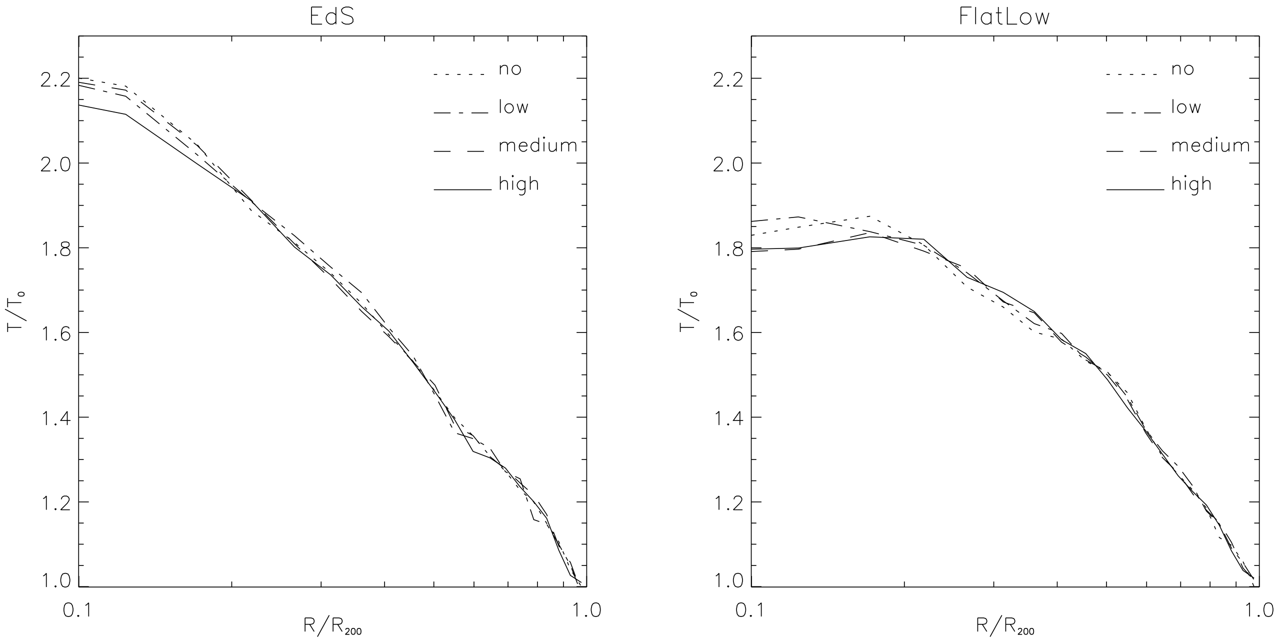


**Fig. 2.** This figure shows the radial temperature profile, averaged across the simulated cluster sample. The temperature is scaled by the mass-weighted temperature of the non-magnetised cluster at a radius of $r_{200}$, and the radius is scaled by $r_{200}$. Different line types distinguish different initial magnetic field strengths, as indicated in the plot. The temperature change with increasing magnetic field strength is clearly visible. The temperature decrease near cluster centres is compatible with the isotropic estimate of eq. (1). As in Fig. 1, the left panel represents the EdS cosmology, the right panel the FlatLow cosmology.

be anisotropic further out. Even though the fraction of the magnetic relative to the thermal pressure, averaged within spherical shells, is approximately constant across the cluster, the detailed effects of magnetic pressure on the gas flow depend on the direction of the magnetic field relative to other locally preferred directions, like the orientation of filaments surrounding a cluster, the local path of matter infall, the orbit of a merging subclump and such. Therefore, the same overall magnetic pressure can have different effects on the local dynamics of gas flows, depending on whether the magnetic field is ordered on scales comparable to the cluster scale, and on the orientation of the magnetic field. In addition, the magnetic field alters the dynamical time scale of a (simulated) cluster. Therefore, when comparing simulated clusters with and without magnetic fields at equal redshifts, we must be aware that we may be comparing them at slightly different evolutionary stages according to their intrinsic timescale.

Figure 2 shows the temperature profile averaged across the set of ten simulated clusters. On the whole, the temperature increases towards the cluster centre by a factor of $\approx 2$. For different cosmologies, the final clusters have a different amount of substructure. This leads to different shapes of the temperature profiles for the clusters in the two different cosmologies used. Although the detailed temperature profile of an individual cluster depends on its dynamical state and formation history, the tendency is clearly visible that the cluster temperature decreases with increasing initial magnetic field strength towards the cluster centre. Deviations from this general trend are possible in individual clusters because of the reasons mentioned before. The mean across the entire cluster sample, however, reveals a monotonic trend increasing towards the cluster centre. This behaviour is expected in view of the previous discussion about the impact of the magnetic field in different parts of the cluster.

### 3.2. Temperature-mass relation

**Table 3.** This table shows the temperature difference between the magnetised and non-magnetised clusters (columns 2 and 4), and the *rms* (columns 3 and 5) of this distribution, for the three different initial magnetic field strengths. Columns 2 and 3 are for the EdS, columns 4 and 5 for the FlatLow cosmologies, respectively. The temperatures are emission-weighted temperatures within the virial radius $r_{200}$. All clusters shown in Figure 1 are used.

| model | $\langle\|\Delta T\|\rangle_{\rm EdS}$ | *rms* | $\langle\|\Delta T\|\rangle_{\rm FlatLow}$ | *rms* |
|---|---|---|---|---|
| low | 4.3% | 2.7% | 2.0% | 2.1% |
| medium | 3.1% | 3.7% | 2.4% | 2.1% |
| high | 5.8% | 5.1% | 2.5% | 1.7% |

The effect of magnetic fields on the temperature-mass relation in galaxy clusters is shown in Fig. 3. Different initial magnetic field strengths are marked with different symbols. As shown before, the effect of the magnetic pressure on the temperature is on

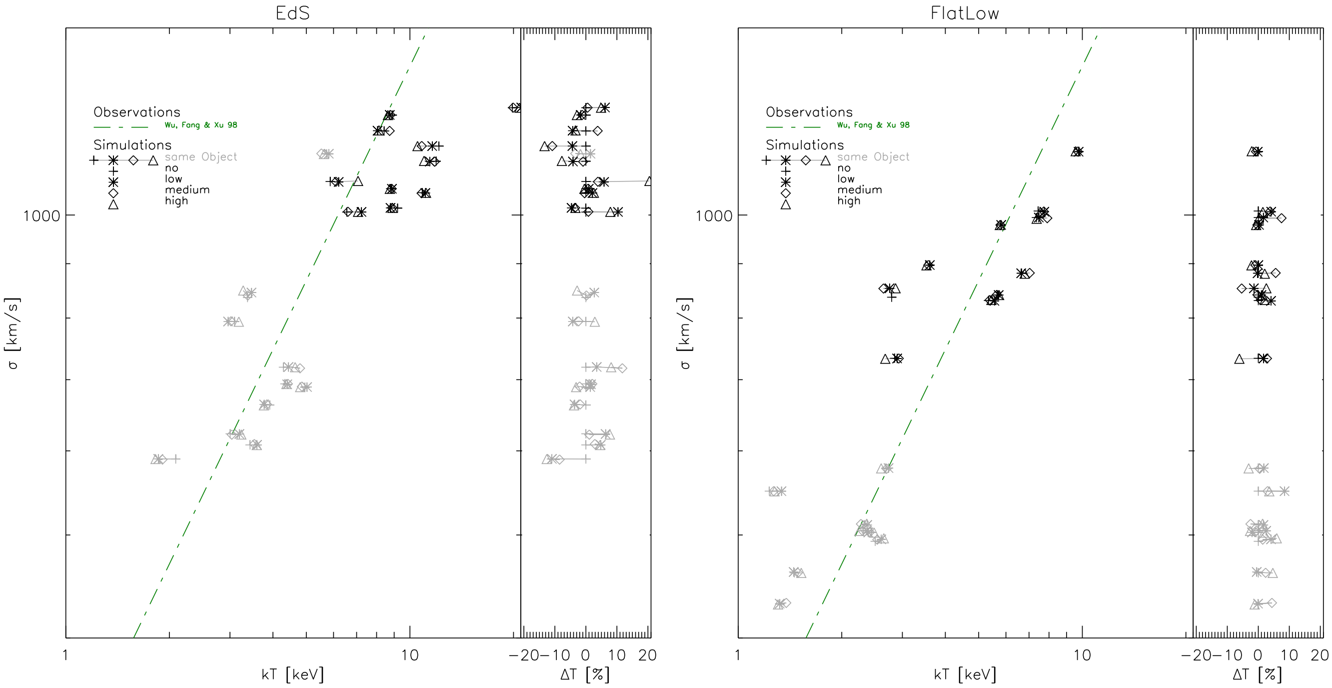


**Fig. 3.** The large panels show the temperature-mass relation for the simulated cluster sample. Here, the temperature is the emission-weighted temperature within the radius $r_{200}$. All clusters are simulated with different initial magnetic field strengths marked by different symbols, as indicated in the plot. The right-hand overlays show the temperature *change* relative to non-magnetised clusters for the different initial magnetic field strengths in percent for each simulated cluster. The large scatter is obvious, but there is a general tendency towards lower temperatures in magnetised clusters. To follow this relation towards lower temperatures, smaller objects (marked as gray symbols) found in the simulations are also used, which lead to a total of 20 different clusters for the EdS cosmology (left panel) and 18 different clusters for the FlatLow cosmology (right panel). As low mass objects are represented by less particles, the resolution in these objects drops towards lower masses and the scatter in these objects is expected to be larger.

average strongest near cluster centres. Therefore, the strength of the effect on the temperature-mass relation depends on the chosen radius within which the mean temperature is calculated. It changes also if we choose the emission-weighted instead of the mass-weighted temperature. For Fig. 3, we have chosen to calculate the emission-weighted temperature within the virial radius $r_{200}$ in order to be comparable to the measurements. We also translated the masses of the simulated galaxy clusters to velocity dispersions. Figure 3 also shows the measured relationship between cluster temperatures and velocity dispersion as dashed-dotted line. The fairly large scatter in individual clusters is clearly seen. In the mean, the temperature difference between the magnetised and non-magnetised clusters is $\approx 5\%$, and it can go up to $10 - 15\%$ in individual clusters.

Although the systematic effect of magnetic fields on the emission-weighted temperature profiles is small, the magnetic fields also increase the scatter in the mass-temperature relation. Values for the *rms* scatter are given in Table 3. This effect is more pronounced in the EdS cosmology because of the smaller gas fraction in a high-density universe.

## 4. Discussion

We tested the influence of the non-thermal pressure support due to magnetic fields in galaxy clusters. Therefore, we performed cosmological MHD simulations of ten clusters in two different cosmologies, each with four different initial magnetic field configurations, thus yielding a total of 80 cluster models.

For initial magnetic field strengths which lead to final fields of $\mu$G strength that reproduce the statistics of observed Faraday-rotation measurements, we found a relatively small non-thermal pressure support of about $5\%$. The temperature change in the cluster cores is therefore on average $\approx 5\%$, with the general tendency towards decreasing temperature with increasing magnetic field strength. This tendency is most pronounced in cosmologies with a low gas fraction, i.e. a high dark-matter density. The effect of the magnetic fields can be substantially stronger in individual clusters, introducing a cosmology-dependent scatter of up to $(10 - 15)\,\%$ into the mass-temperature relation. On the whole, however, our simulations show that realistic magnetic fields in galaxy clusters are dynamically unimportant.

## References


Brio, M., Wo, C.C., 1988, J. Comput. Phys., 75, 400
Dolag, K., Bartelmann, M. Lesch, H., 1999, A&A, 348, 351
Dolag K., Bartelmann M., Lesch H., 2000, in preparation
Dolag, K., Ensslin, T., 2000, in preparation
Kim, K.T., Kronberg, P.P., Tribble, P.C., 1991, ApJ, 379, 80

Kronberg, P.P., 1994, Rep. Prog. Phys., 57, 325
Lucy, L., 1977, AJ, 82, 1013
Monaghan, J.J., 1992, ARA&A, 30, 543
Steinmetz, M., 1996, MNRAS, 278, 1005
Sugimoto, D., Chikada, Y., Makino, J., Ito, T., Ebisuzaki, T., Umemura, M., 1990, Nat, 345, 33
Vallee, J.P., MacLeod, J.M., Broten, N.W., 1986, A&A, 156, 386
Vallee, J.P., MacLeod, J.M., Broten, N.W., 1987, ApL, 25, 181
Wu, X., Fang, L., Xu, W., 1998, A&A, 338, 813